**Saurin Patel**[1]
**Shizhi Qian**[2,3]
**Xiangchun Xuan**[1]

[1]Department of Mechanical Engineering, Clemson University, Clemson, SC, USA
[2]Institute of Micro and Nanotechnology, Old Dominion University , Norfolk, VA, USA
[3]School of Mechanical Engineering, Yeungnam University, Gyongsan, South Korea

Received August 1, 2012
Revised October 5, 2012
Accepted October 5, 2012

Research Article

# Reservoir-based dielectrophoresis for microfluidic particle separation by charge

The separation of particles from a complex mixture is important to a wide range of applications in industry, biology, medicine etc. This work demonstrates a microfluidic approach to separate similar-sized fluorescent and nonfluorescent particles based upon the difference in their surface charges inside a reservoir. Such a separation exploits the reservoir-based dielectrophoresis, which is induced by the inherent electric field gradient formed at the reservoir–microchannel junction, to isolate the trapped fluorescent particles within the reservoir from the streaming nonfluorescent particles. The effects of the DC field magnitude (or equivalently the electrokinetic flow magnitude) and the AC field frequency of DC-biased AC electric fields are investigated on particle separation. A numerical model is also developed to simulate the electrokinetic transport behaviors of the two types of particles. This demonstrated reservoir-based dielectrophoresis particle sorter can operate in parallel to increase the flow throughput. It is suitable for integration with other functional parts into lab-on-a-chip devices for diverse particle handling.

**Keywords:**
Electrokinetics / Microfluidics / Particle separation / Reservoir-based dielectrophoresis / Surface charge
DOI 10.1002/elps.201200467

## 1 Introduction

Separating particles (either synthetic or biological) from a complex mixture is important to a wide range of applications in industry, biology, medicine etc. In the past two decades, microfluidics has evolved to be a very useful tool for particle separation and manipulation in miniaturized devices [1–5]. A variety of microfluidic approaches have so far been developed to separate particles through the use of the force- or flow-field induced electric [6–9], acoustic [10, 11], optical [12, 13], magnetic [14, 15], hydrodynamic [16–18], and inertial [19, 20] particle motions etc. Some of these separations need an extrinsic fluorescent [21] or magnetic [22] labeling of the targeted or nontargeted particles to establish the specificity, which is usually complex and expensive. The rest of the separations, which cover the majority of the demonstrated microfluidic approaches, are label free and based upon the intrinsic particle properties such as size, shape, density, charge, deformability, polarizability (including electric, magnetic, and optical), and compressibility etc. [23].

Surface charge is an important particle property. It determines the particle's electrophoretic mobility and plays an important role in keeping particle suspension dispersed. Charge-based particle separation has been achieved in microfluidic devices using several approaches, which can be classified as batch-wise or continuous flow based on the separation process. The former includes capillary-based electrophoresis [24] and electrical field-flow fractionation [25], where particles of dissimilar charges migrate through a separation column at different times due to their unequal electrophoretic velocities [26] and their residences in stream laminas of unequal velocities [27], respectively. Free-flow electrophoresis is a continuous-flow approach [28], where particles of dissimilar charges are split up into different lanes by their transverse electrophoretic migrations relative to a pressure-driven carrier electrolyte flow [29]. Another continuous-flow microfluidic approach for charge-based particle separation is curvature-induced dielectrophoresis [30], which exploits the inherent electric field gradients within turns [31, 32], to focus and deflect particles to mobility-dependent flow paths in a double-spiral microchannel [33]. Additionally, charge-based particle separation has been demonstrated using a bidirectional flow in a converging–diverging microchannel to trap particles carrying a specific charge [34]. As a net flow was observed experimentally when the particle trapping occurred [35], this separation can be viewed as a continuous-flow approach.

Recently, the authors developed a new microfluidic approach for manipulating particles inside a reservoir. It exploits the particle DEP, that is, induced by the inherent electric field gradient at the reservoir–microchannel junction to focus, trap, and concentrate particles [36] that we termed as reservoir-based dielectrophoresis (rDEP) [37]. This approach

**Correspondence:** Professor Xiangchun Xuan, Department of Mechanical Engineering, Clemson University, Clemson, SC 29634-0921, USA
**E-mail:** xcxuan@clemson.edu
**Fax:** +1-864-656-7299

**Abbreviation: CM**, Clausius—Mossotti; **rDEP**, reservoir-based DEP; **RMS**, root mean square

**Colour Online:** See the article online to view Figs. 1–6 in colour.

 

has been demonstrated to separate polystyrene particles by size [36] and yeast cells by viability [37] in a microfluidic reservoir. The advantage of the rDEP approach is that the particle manipulation takes place completely inside the reservoir, which can thus save the entire microchannel for other purposes and as well facilitates the miniaturization and integration of the device. In this work, we apply such an rDEP approach to microfluidic particle separation based upon surface charge. The factors that may affect the separation are studied. A theoretical model is also developed to understand and predict the electrokinetic particle transport behaviors at the reservoir-microchannel junction during separation.

## 2 Materials and methods

### 2.1 Experimental

#### 2.1.1 Microfluidic device fabrication

The microfluidic device in our experiment was fabricated with PDMS using the standard soft lithography technique. The detailed procedure is given elsewhere [37]. As shown in Fig. 1A, the device is composed of a 1.2-cm-long straight microchannel with a 5 mm-diameter reservoir at each end. The channel is 500 μm wide in the main body and has a constriction section of 50 μm in width and 1 mm in length at the reservoir–microchannel junction in both ends (see the inset in Fig. 1A). These constrictions are designed for the purpose of reducing the applied electric voltage as the electric field can be locally amplified. The channel is uniformly 25 μm deep with a designed radius of 20 μm for all corners.

#### 2.1.2 Particulate solution preparation

To demonstrate the surface charge-based particle separation, we mixed green fluorescent (Bangs Laboratories, Fisher, IN, USA) and nonfluorescent (Sigma-Aldrich, St Louis, MO, USA) polystyrene particles in the ratio of 1:2 and resuspended them in 0.1 mM phosphate buffer to a final concentration of $10^7$–$10^8$ particles per milliliter. Both types of particles are plain particles as per the manufacturers' datasheet and have a diameter of 3 μm while bearing dissimilar surface charges. The latter is evidenced by the discrepancy in their electrokinetic mobility values, which can be experimentally measured and will be presented in Section 2.2.2. Tween 20 (Fisher Scientific, Waltham, MA, USA) was added to the particle solution at 0.1% v/v to suppress the aggregation of particles and their adhesion to channel walls. Prior to use, the particle solution was stirred in a vortex generator to ensure a uniform distribution of each type of particles.

#### 2.1.3 Particle manipulation and visualization

The microchannel and its two reservoirs were primed with the particle-free 0.1 mM phosphate buffer for 10 min. At the beginning of a separation experiment, the buffer solution in the inlet reservoir was vacated using a pipette and replaced with the particle mixture solution. The buffer solution within the microchannel and the outlet reservoir was maintained, which was devoid of particles. Therefore, visual inspection of the outlet reservoir at the end of the experiment could be used to determine the separation purity. Pressure-driven flow was minimized by carefully balancing the liquid heights in the two reservoirs prior to each experiment. The electrokinetic manipulation of the particle mixture in the microfluidic device was attained by imposing DC-biased AC electric fields across the length of the microchannel. The electric fields were supplied by a function generator (33220A, Agilent Technologies, Santa Clara, CA, USA) in conjunction with a high-voltage amplifier (609E-6, Trek, Medina, NY, USA). The frequency of AC field was fixed at 1 kHz in most experiments and was varied from 0.5 to

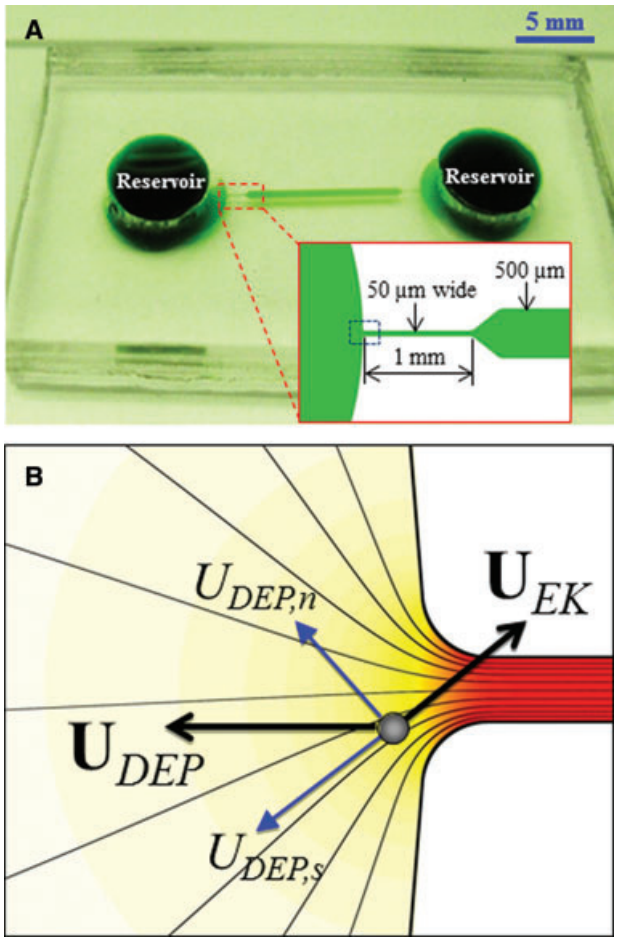


**Figure 1.** (A) Picture of the microfluidic device (filled with green food dye for clarity) used in the experiment. The inset displays a close-up view of the reservoir–microchannel junction with dimensions included. (B) Velocity analysis of a particle at the reservoir–microchannel junction (i.e. the boxed region in the inset of (A)) due to electrokinetic flow and the induced rDEP. The thin lines represent the electric field lines or equivalently fluid streamlines in the absence of the particle. The background color shows the electric field contour (the darker color, the larger field magnitude).

 

5 kHz in examining its influence on particle separation. Higher frequencies were not tested due to the equipment limitation. Particle motion was monitored using an inverted microscope (Nikon Eclipse TE2000U, Nikon Instruments, Lewisville, TX, USA), through which videos (at around 12 frames/s) and images at the reservoir–microchannel junction were recorded using a CCD camera (Nikon DS-Qi1Mc). To visualize the fluorescent and nonfluorescent particles simultaneously, we used a green fluorescent light along with a relatively weak white light to illuminate the reservoir–microchannel junction.

## 2.2 Theory

### 2.2.1 Particle separation mechanism

As illustrated by its contour (the darker color, the larger magnitude) in Fig. 1B, electric field, E, becomes inherently nonuniform at the junction of the reservoir and microchannel (see the boxed region in the inset of Fig. 1A) due to their size mismatch. Therefore, particles experience a dielectrophoretic motion, $U_{DEP}$, when moving electrokinetically through the junction. Using the dipole moment approximation, the time averaged $U_{DEP}$ of an isolated spherical particle under DC and low-frequency (<100 kHz) AC electric fields is given by [38]:

$$U_{DEP} = \frac{\varepsilon_f d^2}{12\eta_f} f_{CM} \nabla E^2 \tag{1}$$

$$f_{CM} = \frac{\sigma_p - \sigma_f}{\sigma_p + 2\sigma_f} \tag{2}$$

where $d$ is the particle diameter, $\varepsilon_f$ is the fluid permittivity, $f_{CM}$ is the so-called Clausius–Mossotti (CM) factor and has been assumed approximately identical for DC and low-frequency (<100 kHz) AC electric fields, $\eta_f$ is the fluid dynamic viscosity, E is the local electric field in root mean square (RMS) value, $\sigma_p$ and $\sigma_f$ are the electric conductivities of the particle and the suspending fluid, respectively. As polymer particles [39] and biological cells [40] often appear poorly conducting in DC and low-frequency AC electric fields, one can have $\sigma_p < \sigma_f$ and, thus, $f_{CM} < 0$ leading to negative DEP [41]. Therefore, $U_{DEP}$ points toward the lower electric field region as indicated by the particle velocity analysis in Fig. 1B.

The observed particle velocity, $U_p$, is the vector addition of the DC electrokinetic motion (a combination of fluid electroosmosis and particle electrophoresis), $U_{EK}$, and the AC/DC dielectrophoretic velocity, $U_{DEP}$:

$$U_p = U_{EK} + U_{DEP} = \mu_{EK} E_{DC} + \mu_{DEP} \nabla E^2 \tag{3}$$

$$\mu_{EK} = f_g \frac{\varepsilon_f (\zeta_p - \zeta_w)}{\eta_f}, \tag{4a}$$

$$\mu_{DEP} = \frac{\varepsilon_f d^2 f_{CM}}{12\eta_f} \tag{4b}$$

where $\mu_{EK}$ is the electrokinetic particle mobility, $E_{DC}$ is the DC component of the applied DC-biased AC electric field, $\mu_{DEP}$ is the dielectrophoretic particle mobility, $f_g$ is the factor that accounts for the wall effects on particle motion and is close to 1 for the particles used in our experiments [42], $\zeta_p$ is the particle zeta potential that is controlled by the surface charge, and $\zeta_w$ is the wall zeta potential. Note that the Brownian, inertial, and gravitational motions of particles have been neglected in Eq. (3), which is reasonable for micron-sized particles in electrokinetic microfluidics [43]. The electrokinetic velocity, $U_{EK}$, is parallel to the electric field lines and hence streamwise due to the similarity of electric and flow field in pure electrokinetics [44]. In contrast, the rDEP velocity, $U_{DEP}$, can have a component in both the streamwise and the cross-stream directions as explained in our earlier works [36, 37]. Therefore, we rewrite Eq. (3) in streamline coordinates as follows:

$$\begin{aligned} U_p &= (U_{EK} + U_{DEP,s})\,\hat{s} + U_{DEP,n}\hat{n} \\ &= \left(\mu_{EK} E_{DC} + \mu_{DEP} \frac{\partial E^2}{\partial s}\right)\hat{s} + \left(2\mu_{DEP} \frac{E^2}{\Re}\right)\hat{n} \end{aligned} \tag{5}$$

where $U_{EK}$ is the magnitude of the electrokinetic velocity, $U_{DEP,s}$ is the magnitude of the streamwise dielectrophoretic particle velocity, $\hat{s}$ is the unit vector of the coordinate $s$ along the streamlines, $U_{DEP,n}$ is the magnitude of the cross-stream dielectrophoretic particle velocity, $\hat{n}$ is the unit vector of the coordinate $n$ normal to the streamlines, and $\Re$ is the local radius of curvature of the streamline. Note that the derivation of the dielectrophoretic velocity terms in Eq. (5) is analogous to that of fluid acceleration in streamline coordinates.

For particles experiencing negative DEP (i.e. $\mu_{DEP} < 0$), $U_{DEP,n}$ is directed toward the centerline of the microchannel (see the velocity analysis in Fig. 1B), which produces a focusing effect on the suspended particles at the reservoir–microchannel junction [36, 37]. Meanwhile, $U_{DEP,s}$ is against the $U_{EK}$ and hence slows down the particle motion at the reservoir–microchannel junction. Moreover, since $U_{DEP,s}$ is a second-order function of the total electric field, $E$, while $U_{EK}$ is linearly proportional to only the DC field component, $E_{DC}$, one can expect $U_{DEP,s}$ to counter-balance $U_{EK}$ at large electric fields, i.e.:

$$\mu_{EK} E_{DC} + \mu_{DEP} \frac{\partial E^2}{\partial s} \le 0 \quad \text{or} \quad \frac{\mu_{EK}}{-\mu_{DEP}} \le 2\left(1+\alpha^2\right) \frac{\partial E_{DC}}{\partial s} \tag{6}$$

where $\alpha$ is the AC to DC field ratio, i.e. $E = E_{DC} + E_{AC} = E_{DC}(1 + \alpha)$. When this happens particles can be stagnated and concentrated at the reservoir–microchannel junction [36, 37]. Such rDEP trapping is dependent on the electrokinetic to dielectrophoretic particle mobility ratio:

$$\frac{\mu_{EK}}{-\mu_{DEP}} = \frac{6 f_g \left(\zeta_p - \zeta_w\right)}{d^2 f_{CM}} \tag{7}$$

which is an explicit function of particle size ($d$) and charge ($\zeta_p$). The larger the mobility ratio is, the more difficult (e.g. a higher AC to DC field ratio, $\alpha$, is required if the DC field is fixed)is to trap the particle. This indicates that we can

 

potentially trap and concentrate one type of particles in the upstream reservoir while sweeping the other type to the downstream reservoir based upon one of these properties. We have recently reported the microfluidic separation of particles by size using rDEP [36]. In this work, we aim to demonstrate the application of rDEP to surface charge-based separation of particles with a similar size.

### 2.2.2 Numerical model and validation

The simulation of electrokinetic particle motion from reservoir to microchannel was conducted in COMSOL 3.5a (Burlington, MA, USA) using a 2D model we developed earlier [45–47]. This model neglects the perturbations of finite-sized particles to the flow and electric fields, which in turn causes errors in the computation of particle velocity. To account for such particle size effects (and other effects as well if any), a correction factor, $\lambda_c$, was introduced to Eq. (3) to correct the dielectrophoretic particle velocity, i.e.:

$$U_p = \mu_{EK} E_{DC} + \lambda_c \mu_{DEP} \left(1 + \alpha^2\right) \nabla E_{DC}^2 \quad (8)$$

The value of $\lambda_c$ spans from 0 to 1 and decreases with the increase of particle size [33, 36, 45–47]. This corrected particle velocity was used as an input to the particle tracing function in COMSOL, where the involving parameters were obtained as follows. The DC electric field component, $E_{DC} = -\nabla\phi_{DC}$, was calculated by solving for the DC electric potential, $\phi_{DC}$, from Laplace equation $\nabla^2\phi_{DC} = 0$. To do so, the electrode in each reservoir was simulated as a 0.5-mm-diameter concentric circle, upon which an electric potential was imposed. Specifically, the experimentally applied DC voltage was imposed to the electrode in the entry reservoir. The electrode in the exit reservoir was grounded. All microchannel walls were assumed to be electrically insulated. Note that the contribution of the AC electric field component to dielectrophoretic particle velocity is considered through the use of the AC to DC field ratio, $\alpha$, in Eq. (8).

The dielectrophoretic particle mobility, $\mu_{DEP}$, in Eq. (8) was calculated from Eq. 4(b) with the typical dynamic viscosity, $\eta_f = 1.0 \times 10^{-3}$ kg/ms and permittivity $\varepsilon_f = 6.9 \times 10^{-10}$ C/vm for pure water at 20°C. To obtain the $f_{CM}$, the electric conductivity of polystyrene particles was computed from $\sigma_p = 4\ K_s/d$ with $K_s = 1$ nS being the recommended value for surface conductance [39], which gave $\sigma_p = 13.3$ μS/cm for $d = 3$ μm particles. Considering the measured electric conductivity of 0.1 mM phosphate buffer, $\sigma_f = 25$ μS/cm, we obtained $f_{CM} = -0.19$ for both the fluorescent and nonfluorescent particles used in our experiment. The electrokinetic particle mobility, $\mu_{EK}$, was determined by tracking the motion of individual particles in the main body of microchannel (where DEP is negligible) under a small pure DC electric field. Specifically, we imposed a 25 V DC voltage across the 1.2-cm long microchannel, which produced an average electric field of about 20 V/cm. At this electric field, Joule heating effects were estimated to be negligible [48, 49]. The resultant electrokinetic velocity of particles in the working buffer was measured in the middle of the channel length, which was then divided by the numerically computed local electric field to give the electrokinetic mobility. We did not perform this test at other electric fields because no significant variations were found among the measurements at different electric fields as long as Joule heating effects are insignificant [50]. We obtained $\mu_{EK} = 5.9 \times 10^{-8}$ m$^2$/Vs and $2.8 \times 10^{-8}$ m$^2$/Vs for the nonfluorescent and fluorescent particles, respectively. In other words, these two types of particles indeed carry different amounts of surface charges, which may be due to the incorporation of dyes into the polymer of the fluorescent particles as suggested by Jellema et al. [34]. From the measured electrokinetic mobility values, we estimate that the average zeta potentials of the nonfluorescent and fluorescent particles are around −20 and −60 mV, respectively, while the average zeta potential of the PDMS/glass channel walls is about −100 mV in 0.1 mM buffer solution [39, 51].

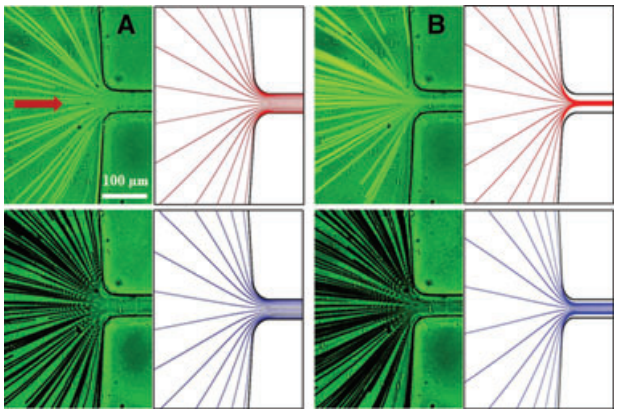


**Figure 2.** Comparison of the experimentally obtained streak images (left column in each panel) and numerically predicted trajectories (right column in each panel) of fluorescent (top row) and nonfluorescent (bottom row) 3 μm particles at the reservoir–microchannel junction under the influence of rDEP. Note that the two types of particles were mixed together in the experiment. The applied DC voltage is fixed at 25 V and the 1-kHz AC voltage (RMS value) is varied from 0 V (A) to 400 V (B). The block arrow in (A) indicates the particle moving direction.

To select the correction factor, $\lambda_c$, in Eq. (8), we compared the simulated trajectories of the two types of particles at the reservoir–microchannel junction with the experimentally obtained particle streak images. Figure 2 shows this comparison for the motion of the particle mixture in two circumstances: one is under 25 V DC and the other is under 25 V DC plus 400 V AC (RMS value, 1 kHz frequency). Note that the streak images of the fluorescent and nonfluorescent particles were each obtained by superimposing the same sequence of over 600 images with respect to the bright and dark bases, respectively. The correction factor was set to 0.8 for both particles, which is consistent with the values for particles and cells of comparable sizes used in our previous studies [31, 33, 36, 37, 46, 47, 52]. On the application of a small pure DC field, fluorescent (top row) and nonfluorescent (bottom row) particles both enter into the microchannel in a uniformly distributed manner because the influence from rDEP is very

 

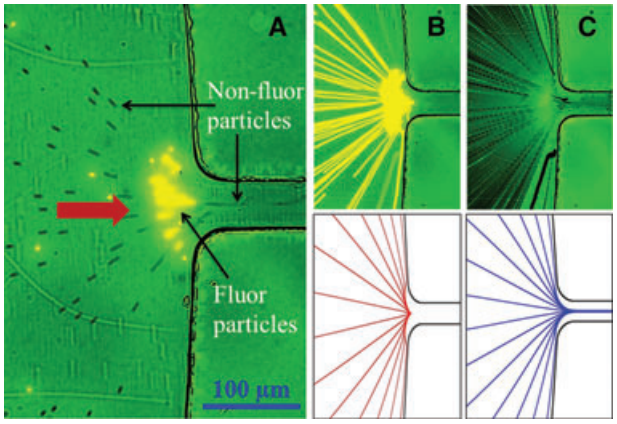


**Figure 3.** Demonstration of surface charge based separation of 3 μm fluorescent particles from 3 μm nonfluorescent particles at the reservoir–microchannel junction by rDEP. (A) A snapshot image of the particle behaviors 45 s after the 50 V DC-biased 800 V AC (RMS value, 1 kHz) voltage was applied. (B and C) The comparison of the experimentally obtained streak images (top row) and the numerically predicted trajectories (bottom row) of the fluorescent and nonfluorescent particles, respectively. The block arrow in (A) indicates the particle moving direction.

weak (Fig. 2A). However, when the AC electric field is added, fluorescent particles (top row, the right image) are focused to a tight stream along the centerline of the microchannel. In contrast, nonfluorescent particles (bottom row, the right image) are much less focused and still cover more than one half of the channel width as seen in Fig. 2B. This discrepancy is attributed to the larger electrokinetic mobility of nonfluorescent particles as presented above. Therefore, fluorescent particles can obtain a greater cross-stream rDEP deflection than nonfluorescent ones do over an equal traveling distance. The simulated trajectories (right columns in Fig. 2A and B) agree closely with the experimental images (left columns) for both particles in both circumstances, which validate the numerical model and verifies the correction factor value as well.

## 3 Results and discussion

### 3.1 Charge-based particle separation using rDEP

Figure 3 demonstrates the surface charge-based separation of 3 μm fluorescent and nonfluorescent particles at the reservoir–microchannel junction using rDEP. It was implemented by applying a 50 V DC biased 800 V AC voltage across the microchannel. The frequency of the AC voltage was maintained at 1 kHz. The magnitude of the computed DC electric field at the junction is about 150 V/cm and that of the local gradient of the DC electric field squared is around $5 \times 10^6$ $V^2/cm^3$. The values of these two quantities for the AC electric field are 2400 V/cm and $1.28 \times 10^9$ $V^2/cm^3$, respectively. Figure 3A shows a snapshot image of the particle behaviors at the junction 45 s after the electric field was turned on. One can see that the fluorescent particles are concentrated inside the reservoir while the nonfluorescent particles can migrate through the junction in a focused stream along the centerline of the microchannel. Such filtering-based particle separations have also been demonstrated using several other dielectrophoretic techniques, for instance, insulator-based DEP [53–55] and contactless DEP [56, 57] as reviewed recently by Srivastava et al. [7], Regtmeier et al. [8], and Cetin and Li [9]. However, most of these separations arise from the particle size difference and none of them is based upon particle surface charge.

The charge-based particle separation that we demonstrate in Fig. 3A happens because the fluorescent particles possess a smaller electrokinetic to dielectrophoretic mobility ratio (see the definition in Eq. (7)) than the nonfluorescent ones and hence can be trapped more easily (see Eq. 6). It is simply a result of the fluorescent particles' lower electrokinetic mobility as measured experimentally (see Section 2.2.2 and also Fig. 2) considering that the two types of particles possess a similar value for dielectrophoretic mobility. The streak images of the fluorescent and nonfluorescent particles are illustrated in the top row of Fig. 3B and C, respectively. Numerically predicted trajectories of these two particles are displayed in the bottom row, and agree with the experimental results. It is, however, important to note that our numerical model can only predict the occurrence of particle trapping due to rDEP at the reservoir–microchannel junction. Since particle–particle interactions and particle effects on fluid flow and electric field are both neglected, this model is unable to simulate the behavior of particles after they get trapped.

The estimated flow rate of this demonstrated charge-based particle separation is 0.25 μL/min, which is more than five times larger than the approach we reported in an earlier work through the use of curvature-induced DEP [33]. It can be easily enhanced by increasing the DC voltage (see Section 3.2) and/or employing a parallel operation (e.g. design multiple microchannels in the radial direction to form a circle about the inlet reservoir). The purity of this separation was examined by visually inspecting both the reservoir–microchannel junction during the experiment and the outlet reservoir after the experiment. We found that fluorescent particles first formed chains and then clusters inside the inlet reservoir and none of them could escape from the trapping zone. This is also confirmed by the nearly absence of fluorescent particles in the outlet reservoir except for the few that were already in the microchannel before the electric field was applied.

However, we observed that once many fluorescent particles concentrated, some of the nonfluorescent particles could also get captured and pulled into the chains of fluorescent particles. This is mainly caused by the increase of rDEP force due to the disturbances of the local electric field from the trapped nonconducting fluorescent particles. It is speculated that the dipole interactions between the two types of particles and those among the nonfluorescent particles themselves [38, 41] may also play a role in this process. Such an issue poses a practical limit on the continuous running time of the separation experiment, which is common in all other filtering-based

 

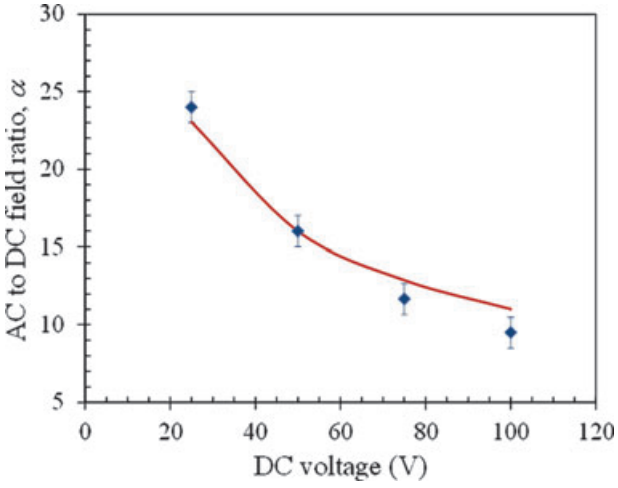


**Figure 4.** Comparison of the experimentally obtained (symbols with error bars) and numerically predicted (curve) AC to DC field ratios, α, for charge-based rDEP separation of 3-μm fluorescent and nonfluorescent particles at the reservoir-microchannel junction at various DC voltages.

separation techniques. This requires the separation to be operated in a semicontinuous manner, i.e. the concentrated fluorescent particles need to be released (by simply reducing the AC field magnitude or increasing the DC field magnitude) once an unacceptable nonfluorescent particle trapping occurs. However, we believe the cycling time of the demonstrated rDEP separation inside a reservoir should be much longer than other reported filtering-based dielectrophoretic separations that all take place within microchannels [7–9]. This is because a reservoir provides a much larger space than a microchannel in both the width and depth directions, and thus can hold a substantially greater number of concentrated particles without a significant contamination. To better understand the phenomenon of the undesired non-fluorescent particle trapping, we experimentally investigated the effects of electrokinetic flow and AC field frequency on the separation, which are presented in Sections 3.2 and 3.3.

### 3.2 Electrokinetic flow effects on particle separation

We conducted the charge-based separation of 3 μm fluorescent and nonfluorescent particles using rDEP at three other DC voltages, which are 25, 75 and 100 V, respectively. As seen from Eq. (6), the increase of DC field should cause a drop in the required AC to DC field ratio, α, for particle trapping. This theoretical prediction is verified by our experiments, which were implemented at 25 V DC/625 V AC ($\alpha = 25$), 50 V DC/800 V AC ($\alpha = 16$), 75 V DC/875 V AC ($\alpha = 11.7$), and 100 V DC/950 V AC ($\alpha = 9.5$), respectively. These experimentally obtained α values (symbols with error bars) agree closely with those predicted from the numerical model (curve) as illustrated in Fig. 4. The snapshot particle images at the reservoir–microchannel junction in these circumstances except for the 75 V DC case (Fig. 6) are presented in Fig. 5.

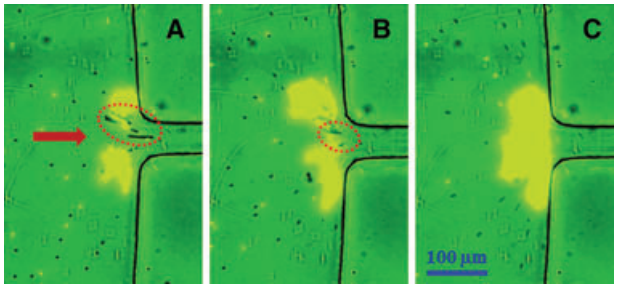


**Figure 5.** Electrokinetic flow effects on charge-based rDEP separation of 3-μm fluorescent and nonfluorescent particles at the reservoir–microchannel junction. Illustrated are the snapshot images taken 2 min after the electric voltage at (A) 25 V DC/625 V AC ($\alpha = 25$), (B) 50 V DC/800 V AC ($\alpha = 16$), and (C) 100 V DC/950 V AC ($\alpha = 9.5$) is imposed to the microchannel. The AC voltages are all in RMS value and at 1 kHz frequency. The dashed lines highlight the regions where nonfluorescent particles are trapped due to the influences from the concentrated fluorescent particles. The block arrow in (A) indicates the particle moving direction.

These images are all taken two min after the electric field is applied. As highlighted by the dashed lines in the images, there are a significant number of nonfluorescent particles trapped along with fluorescent ones at the 25 V DC case in Fig. 5A. This phenomenon, however, diminishes with the increase of the DC voltage as seen in Fig. 5B, and becomes almost invisible at the 100 V DC case in Fig. 5C. It is attributed to the enhanced electrokinetic flow at a higher DC field, which acts to move around the fluorescent particle cluster and drag the nonfluorescent particles into the microchannel in a quicker manner.

### 3.3 AC field frequency effects on particle separation

We also performed the charge-based separation of 3 μm fluorescent and nonfluorescent particles using rDEP under a fixed 75 V DC/875 V AC voltage while at various AC voltage frequencies. Figure 6 compares the snapshot particle images at the reservoir–microchannel junction when the frequency is varied from 0.5 (A) to 1 kHz (B), and 5 kHz (C). All three images were once again taken two min after the application of the electric field. It is evident that the nonselective trapping of nonfluorescent particles becomes more significant with the increase of the AC voltage frequency. Moreover, the particle-trapping zone is greatly expanded at larger frequencies. We do not expect that the variation of AC voltage frequency can affect the rDEP motion of particles to such a considerable extent because the frequency we used in experiments is well below the 100 kHz low-frequency limit [39,40]. It is speculated that the increasing AC voltage frequency greatly enhances the particle-particle interactions [38,41] and hence strengths the trapping of nonfluorescent particles. Additionally as the particles are concentrated near the bottom wall of the microchannel, we speculate that the particle-wall interactions may also contribute to the observed phenomenon in Fig. 6.

 

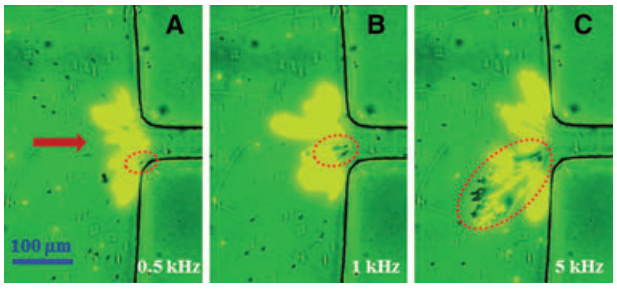


**Figure 6.** AC field frequency effects on charge-based rDEP separation of 3 μm fluorescent and nonfluorescent particles at the reservoir-microchannel junction. Illustrated are the snapshot images taken two min after the application of a 75 V DC-biased 875 V AC voltage (RMS). The AC voltage frequency is varied from 0.5 kHz (A) to 1 kHz (B), and 5 kHz (C). The dashed lines highlight the regions where nonfluorescent particles get trapped due to the influences from the concentrated fluorescent particles. The block arrow in (A) indicates the particle moving direction.

## 4 Concluding remarks

We have applied a recently developed rDEP approach to separate particles based upon surface charge inside a microfluidic reservoir. This separation has been demonstrated through a selective concentration and continuous sorting of 3 μm fluorescent particles from 3 μm nonfluorescent particles under DC-biased AC electric fields. The obtained particle images agree closely with the predicted particle trajectories from a 2D numerical model. It is, however, found that the streaming nonfluorescent particles may also get trapped in the reservoir due to the influences from the accumulated fluorescent particles, which can significantly lower the separation purity. This poses a practical limit on the continuous running time of the separation and requires it to be operated in a semicontinuous manner. The influences from the undesired particle trapping have been found through experiments to decrease with the enhanced electrokinetic flow (by increasing the applied DC electric field) and the lowered AC field frequency. We speculate that besides the tested electric field effects (i.e. DC and AC field magnitudes and AC field frequency), the channel and solution properties (e.g. channel width and depth, corner radius, and solution ionic concentration etc.) can also impact the charge-based particle separation. These factors will be studied in future works. In addition, it is important to note that in principle the rDEP approach can be used to separate any two types of particles of any size as long as they have dissimilar electrokinetic to dielectrophoretic particle mobility ratios. Practically, however, very large electric fields and/or very high AC to DC field ratios will need to be used to realize the separation of very small particles. We are currently working on the manipulation of submicron particles using rDEP.

*This work was supported, in part, by NSF under grant CBET-0853873 (Xuan), by Clemson University through the University Research Grant (Xuan), and by the World Class University Grant (No. R32-2008-000-20082-0) of the Ministry of Education, Science and Technology of Korea (Qian).*

*The authors have declared no conflict of interest.*

## 5 References

[1] Pamme, N., *Lab. Chip.* 2007, *7*, 1644–1659.

[2] Kersaudy-Kerhoas, M., Dhariwal, R., Desmulliez, M. P. Y., *IET Nanobiotechnol.* 2008, *2*, 1–13.

[3] Tsutsui, H., Ho, C. M., *Mech. Res. Commun.* 2009, *36*, 92–103.

[4] Lenshof, A., Laurell, T., *Chem. Soc. Rev.* 2010, *39*, 1203–1217.

[5] Bhagat, A. A. S., Bow, H., Hou, H., Tan, S., Han, J., Lim, C., *Med. Biol. Eng. Comput.* 2010, *48*, 999–1014.

[6] Kang, Y., Li, D., *Microfluid. Nanofluid.* 2009, *6*, 431–460.

[7] Srivastava, S. K., Gencoglu, A., Minerick, A. R., *Anal. Bioanal. Chem.* 2010, *399*, 301–321.

[8] Regtmeier, J., Eichhorn, R., Viefhues, M., Bogunovic, L., Anselmetti, D., *Electrophoresis* 2011, *32*, 2253–2273.

[9] Cetin, B., Li, D., *Electrophoresis* 2011, *32*, 2420–2427.

[10] Laurell, T., Peterson, F., Nilsson, A., *Chem. Soc. Rev.* 2007, *36*, 492–506.

[11] Lin, S. S., Mao, X., Huang, T., *Lab. Chip.* 2012, *12*, 2766–2770.

[12] Wang, M., Tu, E., Raymond, D., Yang, J., Zhang, H., Hagen, N., Dees, B., Mercer, E. M., Forster, A. H., Kariv, I., Marchand, P. J., Butler, W. F., *Nat. Biotechnol.* 2005, *23*, 83–87.

[13] Kim, S. B., Yoon, S. Y., Sung, H. J., Kim, S. S., *Anal. Chem.* 2008, *80*, 2628–2630.

[14] Pamme, N., *Lab. Chip.* 2006, *6*, 24–38.

[15] Gijs, M. A. M., Lacharme, F., Lehmann, U., *Chem. Rev.* 2010, *110*, 1518–1563.

[16] Yamada, M., Nakashima, M., Seki, M., *Anal. Chem.* 2004, *76*, 5465–5471.

[17] Davis, J. A., Inglis, D. W., Morton, K. J., Lawrence, D. A., Huang, L. R., Chou, S. Y., Sturm, J. C., Austin, R. H., *Proc. Natl. Acad. Sci. USA* 2006, *103*, 14779–14784.

[18] Choi, S., Song, S., Choi, C., Park, J. K., *Lab. Chip.* 2007, *7*, 1532–1538.

[19] Di Carlo, D., *Lab. Chip.* 2009, *9*, 3038–3046.

[20] Kuntaegowdanahalli, S., Bhagat, A. A. S., Kumar, G., Papautsky, I., *Lab. Chip.* 2009, *9*, 2973–2980.

[21] Fu, A., Spence, C., Scherer, A., Arnold, F. H., Quake, S. R., *Nat. Biotechnol.* 1999, *17*, 1109–1111.

[22] Adams, J. D., Kim, U., Soh, H. T., *Proc. Natl. Acad. Sci. USA* 2008, *105*, 18165–18170.

[23] Gossett, D. R., Weaver, W. M., Mach, A. J., Hur, S. C., Tse, H. T. K., Lee, W., Amini, H., Di Carlo, D., *Anal. Bioanal. Chem.* 2010, *397*, 3249–3267.

[24] Rodriguez, M. A., Armstrong, D. W., *J. Chromatogr. B* 2004, *800*, 7–25.

[25] Giddings, J. C., *Science* 1993, *206*, 1456–1465.

 

[26] Subirats, X., Blaas, D., Kenndler, E., *Electrophoresis* 2011, *32*, 1579–1590.

[27] Gale, B. K., Caldwell, K. D., Frazier, A. B., *IEEE Trans. Biomed. Eng.* 1998, *45*, 1459–1469.

[28] Krivankova, L., Bocek, P., *Electrophoresis* 1998, *19*, 1064–1074.

[29] Kohlheyer, D., Eijkel, J. C. T., van den Berg, A., Schasfoort, R. B. M., *Electrophoresis* 2008, *29*, 977–993.

[30] Zhu, J., Canter, R. C., Keten, G., Vedantam, P., Tzeng, T. J., Xuan, X., *Microfluid. Nanofluid.* 2011, *11*, 743–752.

[31] Zhu, J., Tzeng, T. J., Hu, G., Xuan, X., *Microfluid. Nanofluid.* 2009, *7*, 751–756.

[32] Zhu, J., Tzeng, T. R., Xuan, X., *Electrophoresis* 2010, *31*, 1382–1388.

[33] Zhu, J., Xuan, X., *Biomicrofluidics* 2011, *5*, 024111.

[34] Jellema, L. C., Mey, T., Koster, S., Verpoorte, E., *Lab. Chip.* 2009, *9*, 1914–1925.

[35] Lettieri, G. L., Dodge, A., Boer, G., de Rooij, N. F., Verpoorte, E., *Lab. Chip.* 2003, *3*, 34–39.

[36] Zhu, J., Hu, G., Xuan, X., *Electrophoresis* 2012, *33*, 916–922.

[37] Patel, S., Showers, D., Vedantam, P., Tzeng, T. J., Qian, S., Xuan, X., *Biomicrofluidics* 2012, *6*, 034102.

[38] Morgan, H., Green, N. G., *AC Electrokinetics: Colloids and Nanoparticles*, Research Studies Press, Hertfordshire, UK 2002.

[39] Ermolina, I., Morgan, H., *J. Colloid Interface Sci.* 2005, *285*, 419–428.

[40] Voldman, J., *Annu. Rev. Biomed. Eng.* 2006, *8*, 425–454.

[41] Jones, T. B., *Electromechanics of Particles*, Cambridge University Press, New York City, NY 1995.

[42] Anderson, J. L., *Annu. Rev. Fluid Mech.* 1989, *21*, 61–99.

[43] Li, D., *Electrokinetics in Microfluidics*, Academic Press, London, 2004.

[44] Cummings, E. B., Griffiths, S. K., Nilson, R. H., Paul, P. H., *Anal. Chem.* 2000, *72*, 2526–2532.

[45] Kang, K., Xuan, X., Kang, Y., Li, D., *J. Appl. Phys.* 2006, *99*, 064702.

[46] Zhu, J., Xuan, X., *Electrophoresis* 2009, *30*, 2668–2675.

[47] Church, C., Zhu, J., Wang, G., Tzeng, T. J., Xuan, X., *Biomicrofluidics* 2009, *3*, 044109.

[48] Xuan, X., *Electrophoresis* 2008, *29*, 33–43.

[49] Sridharan, S., Zhu, J., Hu, G., Xuan, X., *Electrophoresis* 2011, *32*, 2274–2281.

[50] Xuan, X., Raghibizadeh S., Li, D., *J. Colloid Interface Sci.* 2006, *296*, 743–748.

[51] Kirby, B. J., Hasselbrink, E. F. Jr., *Electrophoresis* 2004, *25*, 203–213.

[52] Church, C., Zhu, J., Xuan, X., *Electrophoresis* 2011, *32*, 527–531.

[53] Lapizco-Encinas, B. H., Simmons, B. A., Cummings, E. B., Fintschenko, Y., *Electrophoresis* 2004, *25*, 1695–1704.

[54] Moncada-Hernandez, H., Lapizco-Encinas, B. H., *Anal. Bioanal. Chem.* 2010, *396*, 1805–1816.

[55] Gallo-Villanueva, R. C., Perez-Gonzalez, V. H., Davalos, R. V., Lapizco-Encinas, B. H., *Electrophoresis* 2011, *32*, 2456–2465.

[56] Shafiee, H., Sano, M. B., Henslee, E. A., Caldwell, J. L., Davalos, R. V., *Lab. Chip.* 2010, *10*, 438–445.

[57] Henslee, E. A., Sano, M. B., Rojas, A. D., Schmelz, E. M., Davalos, R. V., *Electrophoresis* 2011, *32*, 2523–2529.

 